


Article

An Approach on Velocity and Stability Control of a Two-Wheeled Robotic Wheelchair

Mostafa Nikpour , Loulin Huang * and Ahmed M. Al-Jumaily 

Institute of Biomedical Technologies, Auckland University of Technology, Auckland 1010, New Zealand; mostafa.nikpour@aut.ac.nz (M.N.); ahmed.aljumaily@aut.ac.nz (A.M.A.-J.)

* Correspondence: loulin.huang@aut.ac.nz

Received: 28 July 2020; Accepted: 10 September 2020; Published: 16 September 2020



Abstract: Conventional robotic wheelchairs (three or four-wheeled) which are statically stable are poor in mobility. Though a two-wheeled robotic wheelchair has better mobility, it is not statically stable and needs an active stability controller. In addition to mobility and stability, velocity control is also important for the operation of a wheelchair. Conventional stability and velocity controllers rely on the motion of the wheels and require high driving torque and power. In this paper, this problem is tackled by adding a compact pendulum-like movable mechanism whose main function is for stability control. Its motion and those of the wheels are controlled through a quasi-sliding mode control approach to achieve a simultaneous velocity and stability control with much less driving torque and power. Simulation results are presented to show the effectiveness of the proposed controller.

Keywords: two-wheeled robotic wheelchair; stability control; velocity control; quasi-sliding mode control

1. Introduction

Compared to conventional manually operated wheelchairs, motorized wheelchairs equipped with an automatic control system (so-called robotic wheelchairs) have many advantages. For example, they have better navigation capabilities and can respond to different motion requirements autonomously [1–3]. Most conventional robotic wheelchairs contain two active driving wheels and two passive casters [4]. Though casters enhance the stability of the wheelchair, they have a negative effect on its mobility [5–7]. To solve this problem, caster-free two-wheeled robotic wheelchair equipped with an active stability controller was proposed [8–10].

There are several types of two-wheeled wheelchairs with special features. The iBot has four wheels, but can be converted to a two-wheeled wheelchair by lifting up its two caster wheels [11–13]. The height of the rider seat increases as a result. A patented iBalanceTM technology, a synthesis of computers and gyroscope, is used to keep the wheelchair stable. A two-wheeled transportation vehicle called B2 has a self-balancing (stability) capability when it is subject to disturbances from the road. It is suitable for use on narrow roads as it can turn on the spot in a space much smaller than that needed by a conventional car [14,15].

Nonlinear controllers can be used for velocity and stability control of a two-wheeled wheelchair as its dynamic model is highly nonlinear [16]. One example is computed torque control based on nonlinear feedback and the assumption that the exact dynamic model of the system is known [17]. For the cases where the system dynamics cannot be accurately modelled, or there are external disturbances, H_∞ which is robust against disturbances can be used [18,19]. Nonlinear H_∞ control is developed based on the Hamilton–Jacobi–Bellman–Isaacs (HJBI) equation which is hard to solve in real-time though [20].

Another type of robust controller is sliding mode control (SMC) which has an elegant structure and is effective in disturbance rejection and is robust to system parameters variation. In this controller, the state of the closed-loop system is forced to slide along the predefined sliding surface [21–23]. However, it suffers chattering in the closed-loop system states. This problem can be solved by quasi-sliding mode control (QSMC) where the non-smooth sign function used in SMC is replaced with a smooth sigmoid function to govern the switching behavior in the controller [24]. For a system whose number of inputs is less than the number of outputs (underactuated system), hierarchical sliding mode control (HSMC) can be used. In HSMC, the sliding surfaces are designed in layers which are called layer sliding surface [25].

In most controllers, the motion and stability of the wheelchair all rely on the motions of the driving wheels which need large driving torque and power [26]. Some approaches have been proposed to solve this problem. For example, the rider's seat is made to move to enhance the wheelchair's stability [27]. The wheelchair is designed in a way such that its center of gravity is under the driving wheels' axis [28]. A mass under the rider's seat moves linearly to keep the wheelchair from overturning [29]. These approaches have the drawbacks of compromising the comfort of the rider or limited effectiveness.

In this paper, an active velocity and stability controller is developed for a two-wheeled wheelchair added with a compact pendulum-like movable mechanism. The Euler–Lagrange equation is used to derive the equation of motion (EOM) of the system and a quasi-sliding mode control approach is used in the controller design. Through the proposed control scheme, the wheelchair's velocity and stability can be controlled with driving torque and power much less than those of conventional controllers which only rely on the motions of the driving wheels. Simulation results prove the effectiveness of the proposed controller.

The rest of the paper is organized as follows. In Section 2, the structure of a two-wheeled robotic wheelchair and proposed mechanism is presented. The dynamic model of the system is introduced in Section 3. In Section 4, the controller design is proposed. In Section 5, simulation results are shown to compare the performances of the conventional and proposed methods. Conclusions are given in Section 6.

2. System Description

As shown in Figure 1, a two-wheeled wheelchair comprises a seat and two wheels. The seat is connected to the axial of the wheels through a rod. A pendulum like movable mechanism is connected to the rod through a rotating joint. There is a mass placed at the end of the pendulum. The masses of the pendulum and the rod are ignored. To describe the state of all the modules of the wheelchair, a body coordinate frame X - Y - Z is placed at the center of the wheels' axle (O). Though Z axis is not shown in the figure, it is perpendicular to X and Y axis as determined by the right-hand rule. All moments of inertia are defined around their centre of gravity (CoG) in Z axis. The rotation angles of the wheels and the wheelchair body are measured from Y axis, while the rotation angle of the movable mechanism is measured from link OP . The nomenclature can be found in Table 1.

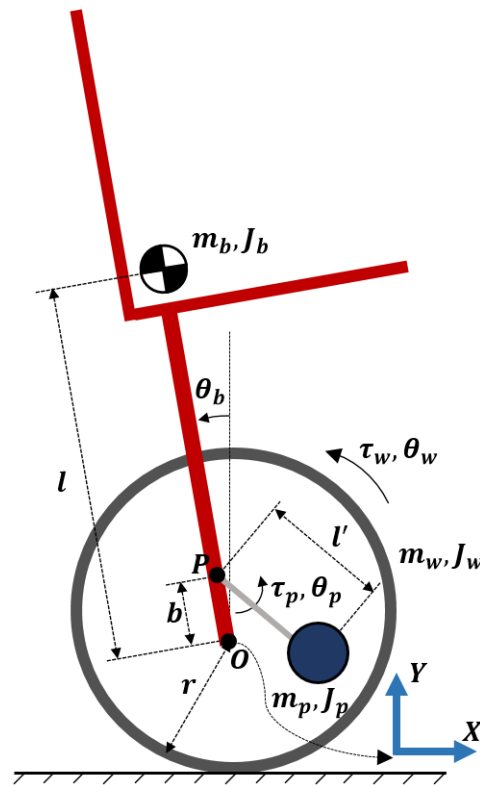


Figure 1. Two-wheeled wheelchair and proposed mechanism.

Table 1. Nomenclature.

Symbol	Description
m_w	Mass of each wheel
m_b	Mass of body
m_p	Mass of movable mechanism
J_w	Moment of inertia of each wheel
J_b	Moment of inertia of body
J_p	Moment of inertia of movable mechanism
O	Centre of the wheels' axle
P	Contact point of the movable mechanism and wheelchair
r	Radius of each wheel
l	Distance from the body's CoG to point P
l'	Length of the rod of the pendulum (movable mechanism)
b	Distance from point O to point P
θ_w	Rotation angle of the wheel
θ_b	Rotation angle of the body (pitch angle)
θ_p	Rotation angle of the pendulum
τ_r	Input torque of the right wheel
τ_l	Input torque of the left wheel
τ_w	Total input torque of the wheels
τ_p	Input torque of the pendulum
P_w	Input power of the wheels
P_p	Input power of the pendulum

3. Modeling of Two-Wheeled Robotic Wheelchair

3.1. Conventional Method

In a conventional method, the wheels are responsible for both the stability and velocity control of the wheelchair. The controller is based on the EOM of the system which can be derived from the Euler–Lagrange equation [30]:

$$\frac{d}{dt}\left(\frac{\partial T}{\partial \dot{q}_i}\right) - \frac{\partial T}{\partial q_i} + \frac{\partial U}{\partial q_i} = Q_i \quad (1)$$

T and U are the kinetic and the potential energy of the system. q_i and Q_i are the generalized coordinates and the corresponding input of system respectively. Slip between the ground and wheels and friction forces in the system are neglected. Each wheel's kinetic and potential energy can be shown as

$$T_w = \frac{1}{2}m_w r^2 \dot{\theta}_w^2 + \frac{1}{2}J_w \dot{\theta}_w^2, \quad U_w = 0.$$

The body's kinetic and potential energy are

$$T_b = \frac{1}{2}m_b r^2 \dot{\theta}_w^2 + \frac{1}{2}m_b l^2 \dot{\theta}_b^2 + m_b r l \dot{\theta}_w \dot{\theta}_b \cos \theta_b + \frac{1}{2}J_b \dot{\theta}_b^2, \quad U_b = m_b g l \cos \theta_b.$$

The overall kinetic and potential energy of the system is

$$T = 2T_w + T_b, \quad U = 2U_w + U_b.$$

Through Equation (1), the EOM of the system can be derived and presented as [31]

$$\mathbf{M}(\mathbf{q})\ddot{\mathbf{q}} + \mathbf{H}(\mathbf{q}, \dot{\mathbf{q}}) + \mathbf{G}(\mathbf{q}) = \mathbf{Q}, \quad (2)$$

where \mathbf{q} is the vector of generalized coordinates

$$\mathbf{q} = \begin{bmatrix} \theta_b & \theta_w \end{bmatrix}^T,$$

$\mathbf{M}(\mathbf{q})$ is the symmetric inertia matrix.

$$\mathbf{M}(\mathbf{q}) = \begin{bmatrix} m_b l^2 + J_b & m_b r l \cos \theta_b \\ m_b r l \cos \theta_b & (2m_w + m_b)r^2 + 2J_w \end{bmatrix},$$

$\mathbf{H}(\mathbf{q}, \dot{\mathbf{q}})$ is the Centrifugal and Coriolis forces matrix.

$$\mathbf{H}(\mathbf{q}, \dot{\mathbf{q}}) = \begin{bmatrix} 0 & -m_b r l \dot{\theta}_b^2 \sin \theta_b \end{bmatrix}^T,$$

$\mathbf{G}(\mathbf{q})$ is the gravity matrix

$$\mathbf{G}(\mathbf{q}) = \begin{bmatrix} -m_b g l \sin \theta_b & 0 \end{bmatrix}^T,$$

and \mathbf{Q} is the corresponding input.

$$\mathbf{Q} = \begin{bmatrix} 0 & \tau_w \end{bmatrix}^T,$$

τ_w is the total torque applied to the right and left wheels,

$$\tau_w = \tau_r + \tau_l.$$

Assuming the same amount of torque applied at each wheel,

$$\tau_r = \tau_l.$$

Then, the input power of the wheel motors is [32]

$$P_w = \tau_w \dot{\theta}_w.$$

Equation (2) is valid when no disturbance is applied to the wheelchair. The effect of disturbances like parameter uncertainties of the wheelchair due to the varying mass of the body can be considered in Equation (2) which reformulate it to

$$\hat{\mathbf{M}}(\mathbf{q})\ddot{\mathbf{q}} + \hat{\mathbf{H}}(\mathbf{q}, \dot{\mathbf{q}}) + \hat{\mathbf{G}}(\mathbf{q}) + \mathbf{D} = \mathbf{Q} \quad (3)$$

where \mathbf{D} denotes the effect of parameter uncertainties in dynamic model of the wheelchair. $\hat{\mathbf{M}}(\mathbf{q})$, $\hat{\mathbf{H}}(\mathbf{q}, \dot{\mathbf{q}})$, $\hat{\mathbf{G}}(\mathbf{q})$ denote the nominal Inertia, centrifugal, and gravity matrices, respectively which can be presented as

$$\hat{\mathbf{M}}(\mathbf{q}) = \mathbf{M}(\mathbf{q}) - \Delta\mathbf{M}(\mathbf{q}), \quad \hat{\mathbf{H}}(\mathbf{q}, \dot{\mathbf{q}}) = \mathbf{H}(\mathbf{q}, \dot{\mathbf{q}}) - \Delta\mathbf{H}(\mathbf{q}, \dot{\mathbf{q}}), \quad \hat{\mathbf{G}}(\mathbf{q}) = \mathbf{G}(\mathbf{q}) - \Delta\mathbf{G}(\mathbf{q})$$

The effect of parameter uncertainties disturbance caused by the mass of body variation can be shown as

$$\mathbf{D} = \Delta\mathbf{M}(\mathbf{q})\ddot{\mathbf{q}} + \Delta\mathbf{H}(\mathbf{q}, \dot{\mathbf{q}}) + \Delta\mathbf{G}(\mathbf{q}) \quad (4)$$

where

$$\Delta\mathbf{M}(\mathbf{q}) = \begin{bmatrix} \Delta m_b l^2 & \Delta m_b r l \cos \theta_b \\ \Delta m_b r l \cos \theta_b & \Delta m_b r^2 \end{bmatrix},$$

$$\Delta\mathbf{H}(\mathbf{q}, \dot{\mathbf{q}}) = \begin{bmatrix} 0 & -\Delta m_b r l \dot{\theta}_b^2 \sin \theta_b \end{bmatrix}^T, \quad \Delta\mathbf{G}(\mathbf{q}) = \begin{bmatrix} -\Delta m_b g l \sin \theta_b & 0 \end{bmatrix}^T.$$

The mass of body uncertainty is shown by $\Delta m_b = m_b - \hat{m}_b$. m_b and \hat{m}_b denote the real and nominal values of mass of body, respectively.

3.2. Proposed Method

In the proposed method, a pendulum-like movable mechanism is added to the wheelchair to mainly assist stability control. Its kinetic and potential energy can be shown as

$$T_p = \frac{1}{2} m_p [r^2 \dot{\theta}_w^2 + b^2 \dot{\theta}_b^2 + 2rb \dot{\theta}_b \dot{\theta}_w \cos \theta_b + l'^2 (\dot{\theta}_b + \dot{\theta}_p)^2 - 2rl' \dot{\theta}_w (\dot{\theta}_b + \dot{\theta}_p) \cos(\theta_b + \theta_p) - 2bl' \dot{\theta}_b (\dot{\theta}_b + \dot{\theta}_p) \cos \theta_p] + \frac{1}{2} J_p (\dot{\theta}_b + \dot{\theta}_p)^2,$$

$$U_p = m_p g (b \cos \theta_b - l' \cos(\theta_p + \theta_b)).$$

Then, the overall kinetic and potential energy of system is derived,

$$T = 2T_w + T_b + T_p, \quad U = 2U_w + U_b + U_p.$$

The EOM of the system derived through Equation (1) is similar to Equation (2) where

$$\mathbf{q} = \begin{bmatrix} \theta_b & \theta_w & \theta_p \end{bmatrix}^T, \quad \mathbf{M}(\mathbf{q}) = \begin{bmatrix} M_{11} & M_{12} & M_{13} \\ M_{21} & M_{22} & M_{23} \\ M_{31} & M_{32} & M_{33} \end{bmatrix}, \quad \mathbf{H}(\mathbf{q}, \dot{\mathbf{q}}) = \begin{bmatrix} H_1 & H_2 & H_3 \end{bmatrix}^T$$

$$\mathbf{G}(\mathbf{q}) = \begin{bmatrix} G_1 & G_2 & G_3 \end{bmatrix}^T, \quad \mathbf{Q} = \begin{bmatrix} 0 & \tau_w & \tau_p \end{bmatrix}^T.$$

The details of the terms $\mathbf{M}(\mathbf{q})$, $\mathbf{H}(\mathbf{q}, \dot{\mathbf{q}})$ and $\mathbf{G}(\mathbf{q})$ matrices can be found in Appendix A. The input power of the motor driving the pendulum is

$$P_p = \tau_p \dot{\theta}_p.$$

The effect of mass of body uncertainty can be shown as Equation (4), where,

$$\Delta \mathbf{M}(\mathbf{q}) = \begin{bmatrix} \Delta m_b l^2 & \Delta m_b r l \cos \theta_b & 0 \\ \Delta m_b r l \cos \theta_b & \Delta m_b r^2 & 0 \\ 0 & 0 & 0 \end{bmatrix},$$

$$\Delta \mathbf{H}(\mathbf{q}, \dot{\mathbf{q}}) = \begin{bmatrix} 0 & -\Delta m_b r l \dot{\theta}_b^2 \sin \theta_b & 0 \end{bmatrix}^T, \quad \Delta \mathbf{G}(\mathbf{q}) = \begin{bmatrix} -\Delta m_b g l \sin \theta_b & 0 & 0 \end{bmatrix}^T.$$

4. Controller Design

4.1. Conventional Method

The control aim is to make the wheelchair move at a desired velocity and keep stable (the pitch angle is around zero). There are two controlled variables (velocity and pitch angle), but there is only one control input (τ_w). This problem can be resolved through a HSMC controller. To design the controller, the following two sliding mode surfaces are defined,

$$\sigma_1 = c_1 e_1 + e_2, \quad \sigma_2 = c_2 e_3 + e_4, \quad (5)$$

where σ_1 and σ_2 are the sliding surfaces for pitch angle and wheel rotational angle respectively. c_1 and c_2 are positive constants. e_1, e_2, e_3 and e_4 are the tracking errors defined according to

$$e_1 = \theta_b - \theta_{b_d}, \quad e_2 = \dot{\theta}_b - \dot{\theta}_{b_d}, \quad e_3 = \theta_w - \theta_{w_d}, \quad e_4 = \dot{\theta}_w - \dot{\theta}_{w_d},$$

where $\theta_{b_d}, \dot{\theta}_{b_d}, \theta_{w_d}$ and $\dot{\theta}_{w_d}$ are the desired values of pitch angle, pitch angular velocity, wheel angle and wheel angular velocity respectively. Differentiating Equation (5) with respect to time leads to

$$\dot{\sigma}_1 = c_1 e_2 + \ddot{\theta}_b - \ddot{\theta}_{b_d}, \quad \dot{\sigma}_2 = c_2 e_4 + \ddot{\theta}_w - \ddot{\theta}_{w_d}. \quad (6)$$

From Equation (2), we have

$$\ddot{\mathbf{q}} = \mathbf{M}^{-1}(\mathbf{q})(-\mathbf{H}(\mathbf{q}, \dot{\mathbf{q}}) - \mathbf{G}(\mathbf{q}) + \mathbf{Q}). \quad (7)$$

Then, we have

$$\begin{cases} \ddot{\theta}_b = -M_{11}^{-1}(H_1 + G_1) - M_{12}^{-1}(H_2 + G_2 - \tau_w) \\ \ddot{\theta}_w = -M_{21}^{-1}(H_1 + G_1) - M_{22}^{-1}(H_2 + G_2 - \tau_w). \end{cases} \quad (8)$$

From Equations (6) and (8), we have

$$\begin{cases} \dot{\sigma}_1 = c_1 e_2 - M_{11}^{-1}(H_1 + G_1) - M_{12}^{-1}(H_2 + G_2 - \tau_w) - \ddot{\theta}_{b_d}, \\ \dot{\sigma}_2 = c_2 e_4 - M_{21}^{-1}(H_1 + G_1) - M_{22}^{-1}(H_2 + G_2 - \tau_w) - \ddot{\theta}_{w_d}. \end{cases} \quad (9)$$

Let $\dot{\sigma}_1 = 0$ and $\dot{\sigma}_2 = 0$, the equivalent control input for each sliding surface can be obtained as

$$\begin{cases} \tau_{w_1} = [-c_1 e_2 + M_{11}^{-1}(H_1 + G_1) + M_{12}^{-1}(H_2 + G_2) + \ddot{\theta}_{b_d}] / M_{12}^{-1}, \\ \tau_{w_2} = [-c_2 e_4 + M_{21}^{-1}(H_1 + G_1) + M_{22}^{-1}(H_2 + G_2) + \ddot{\theta}_{w_d}] / M_{22}^{-1}. \end{cases} \quad (10)$$

To make sure that all tracking errors converge to zero, the control input can be set as [25]

$$\tau_w = \tau_{w_1} + \tau_{w_2} + \tau_{w_s}, \quad (11)$$

where τ_{w_s} is the switching control input in the reaching phase. To obtain τ_{w_s} , a sliding surface is designed as

$$\sigma_s = \alpha \sigma_1 + \beta \sigma_2, \quad (12)$$

where α and β are constants. The τ_{w_s} can be obtained based on Lyapunov stability theorem. Choose a Lyapunov function candidate as

$$V_1 = \frac{1}{2} \sigma_s^2. \quad (13)$$

Differentiating V_1 with respect to time, we have

$$\dot{V}_1 = \sigma_s \dot{\sigma}_s = \sigma_s (\alpha \dot{\sigma}_1 + \beta \dot{\sigma}_2). \quad (14)$$

From Equations (9) and (14), we have

$$\begin{aligned} \dot{V}_1 &= \sigma_s \alpha [c_1 e_2 - M_{11}^{-1}(H_1 + G_1) - M_{12}^{-1}(H_2 + G_2 - \tau_w) - \ddot{\theta}_{b_d}] + \sigma_s \beta [c_2 e_4 - M_{21}^{-1}(H_1 + G_1) \\ &\quad - M_{22}^{-1}(H_2 + G_2 - \tau_w) - \ddot{\theta}_{w_d}] = \sigma_s [\alpha M_{12}^{-1}(\tau_w - \tau_{w_1}) + \beta M_{22}^{-1}(\tau_w - \tau_{w_2})] \\ &= \sigma_s [\alpha M_{12}^{-1}(\tau_{w_s} + \tau_{w_2}) + \beta M_{22}^{-1}(\tau_{w_s} + \tau_{w_1})]. \end{aligned} \quad (15)$$

Select the exponential sliding mode

$$\dot{\sigma}_s = -k_1 \text{sign}(\sigma_s) - k_2 \sigma_s = \alpha M_{12}^{-1}(\tau_{w_s} + \tau_{w_2}) + \beta M_{22}^{-1}(\tau_{w_s} + \tau_{w_1}), \quad (16)$$

where k_1 and k_2 are positive constants. From Equation (16), τ_{w_s} can be obtained as

$$\tau_{w_s} = \frac{-k_1 \text{sign}(\sigma_s) - k_2 \sigma_s - \alpha M_{12}^{-1} \tau_{w_2} - \beta M_{22}^{-1} \tau_{w_1}}{\alpha M_{12}^{-1} + \beta M_{22}^{-1}}. \quad (17)$$

According to the Lyapunov theorem, the below condition should be satisfied to provide stability of HSMC controller [33].

$$\dot{V}_1 < 0 \quad \text{for } \sigma_s \neq 0.$$

From Equations (14) and (16), we have

$$\dot{V}_1 = \sigma_s \dot{\sigma}_s = -k_1 |\sigma_s| - k_2 \sigma_s^2 < 0 \quad \text{for } \sigma_s \neq 0. \quad (18)$$

Equation (18) proves that the sliding surface σ_s is asymptotically stable. The trajectory of the second-layer sliding surface σ_s will converge to the origin of coordinate system constructed by σ_1 and σ_2 axis when $t \rightarrow \infty$. Therefore, each subsystem states move on the first-layer sliding surfaces (σ_1 and σ_2) and we have [34]

$$\lim_{t \rightarrow \infty} \sigma_1 = 0 \quad \lim_{t \rightarrow \infty} \sigma_2 = 0. \quad (19)$$

Equation (19) proves that the first-layer sliding surfaces σ_1 and σ_2 are also asymptotically stable.

4.2. Proposed Method

In the proposed method where a pendulum like movable mechanism is added to the wheelchair, the number of control inputs (τ_w and τ_p) is equal to the number of controlled variables. A QSMC control scheme is suitable in this case. To develop the QSMC controller for the system, the two sliding surfaces σ_1 and σ_2 defined in Equation (5) are used. According to Equation (7), we have

$$\begin{cases} \ddot{\theta}_b = -M_{11}^{-1}(H_1 + G_1) - M_{12}^{-1}(H_2 + G_2 - \tau_w) - M_{13}^{-1}(H_3 + G_3 - \tau_p) \\ \ddot{\theta}_w = -M_{21}^{-1}(H_1 + G_1) - M_{22}^{-1}(H_2 + G_2 - \tau_w) - M_{23}^{-1}(H_3 + G_3 - \tau_p). \end{cases} \quad (20)$$

Combining Equations (6) and (20) yields

$$\begin{cases} \dot{\sigma}_1 = c_1 e_2 - M_{11}^{-1}(H_1 + G_1) - M_{12}^{-1}(H_2 + G_2 - \tau_w) - M_{13}^{-1}(H_3 + G_3 - \tau_p) - \ddot{\theta}_{b_d}, \\ \dot{\sigma}_2 = c_2 e_4 - M_{21}^{-1}(H_1 + G_1) - M_{22}^{-1}(H_2 + G_2 - \tau_w) - M_{23}^{-1}(H_3 + G_3 - \tau_p) - \ddot{\theta}_{w_d}. \end{cases} \quad (21)$$

Note, to avoid the chattering phenomenon, a smooth sigmoid function is replaced with the non-smooth function $\text{sign}(\sigma)$. To obtain equivalent control inputs, $\dot{\sigma}_1$ and $\dot{\sigma}_2$ are considered as

$$\dot{\sigma}_1 = -\rho_1 \frac{\sigma_1}{|\sigma_1| + \varepsilon_1}, \quad \dot{\sigma}_2 = -\rho_2 \frac{\sigma_2}{|\sigma_2| + \varepsilon_2}, \quad (22)$$

where ρ_1 and ρ_2 are two positive controller gains and ε_1 and ε_2 are two small positive scalars [33]. Therefore, the control inputs can be obtained as

$$\begin{cases} \tau_w = (F_1 - \frac{M_{13}^{-1}}{M_{23}^{-1}} F_2) / (M_{12}^{-1} - \frac{M_{22}^{-1} M_{13}^{-1}}{M_{23}^{-1}}), \\ \tau_p = (F_1 - M_{12}^{-1} \tau_w) / M_{13}^{-1}, \end{cases} \quad (23)$$

where

$$\begin{cases} F_1 = -\rho_1 \frac{\sigma_1}{|\sigma_1| + \varepsilon_1} - c_1 e_2 + M_{11}^{-1}(H_1 + G_1) + M_{12}^{-1}(H_2 + G_2) + M_{13}^{-1}(H_3 + G_3) + \ddot{\theta}_{b_d}, \\ F_2 = -\rho_2 \frac{\sigma_2}{|\sigma_2| + \varepsilon_2} - c_2 e_4 + M_{21}^{-1}(H_1 + G_1) + M_{22}^{-1}(H_2 + G_2) + M_{23}^{-1}(H_3 + G_3) + \ddot{\theta}_{w_d}. \end{cases}$$

To prove the stability of the QSMC controller, the Lyapunov function candidates can be chosen as

$$V_2 = \frac{1}{2} \sigma_1^2, \quad V_3 = \frac{1}{2} \sigma_2^2. \quad (24)$$

The below conditions should be satisfied to provide stability of QSMC controller [33].

$$\dot{V}_2 < 0 \quad \text{for } \sigma_1 \neq 0 \quad \dot{V}_3 < 0 \quad \text{for } \sigma_2 \neq 0.$$

From Equations (22) and (24), we have

$$\begin{cases} \dot{V}_2 = \sigma_1 \dot{\sigma}_1 = -\rho_1 \frac{\sigma_1^2}{|\sigma_1| + \varepsilon_1} < 0 \quad \text{for } \sigma_1 \neq 0 \\ \dot{V}_3 = \sigma_2 \dot{\sigma}_2 = -\rho_2 \frac{\sigma_2^2}{|\sigma_2| + \varepsilon_2} < 0 \quad \text{for } \sigma_2 \neq 0. \end{cases}$$

Therefore, the stability of the QSMC controller is guaranteed.

5. Simulation Results

In this section, the performances of the stability and velocity control of a two-wheeled robotic wheelchair through the conventional and the proposed methods are simulated and compared. A two-wheeled robotic wheelchair used in [8] is considered for dynamic modelling and controller design. The physical parameters of the wheelchair and the added pendulum-like movable mechanism can be found in Table 2.

Table 2. Physical parameters of the two-wheeled robotic wheelchair and movable mechanism for simulation.

Property	m_w	\hat{m}_b	m_p	J_w	J_b	J_p	r	l	l'	b
Value	16	48	15.45	0.64	0	0.19	0.26	0.3	0.2	0
Unit	kg	kg	kg	kg · m ²	kg · m ²	kg · m ²	m	m	m	m

5.1. Case 1

In Case 1, the initial values for pitch angle, wheel's rotational angle and the rotational angle of the pendulum angles are respectively set as

$$\theta_{b_0} = 0.2 \text{ rad}, \quad \dot{\theta}_{b_0} = 0, \quad \theta_{w_0} = 0, \quad \dot{\theta}_{w_0} = 0, \quad \theta_{p_0} = 0, \quad \dot{\theta}_{p_0} = 0.$$

According to the control objectives, the desired pitch angle and angular velocity are set to be zero.

$$\theta_{b_d} = 0, \quad \dot{\theta}_{b_d} = 0.$$

The desired angular velocity of the wheels (for the motion along a straight line) is set to be constant. $\dot{\theta}_{w_d} = 20 \text{ rad/s}$. Therefore, the angle as the function of time t can be expressed as $\theta_{w_d} = 20t \text{ rad}$. The control parameters for the HSMC controller are chosen as

$$c_1 = 1.5, \quad c_2 = 0.05, \quad \alpha = 1, \quad \beta = 0.03, \quad k_1 = 1, \quad k_2 = 0.36.$$

The control parameters for the QSMC controller were set as

$$c_1 = 1, \quad c_2 = 0.4, \quad \rho_1 = 0.2, \quad \rho_2 = 0.2, \quad \varepsilon_1 = 0.05, \quad \varepsilon_2 = 0.05.$$

The above control parameters are selected from several sets of parameters based on the performance of the system responses include the accuracy and the speed of the angle and the velocity tracking and the magnitude of the motor's output torque and power within their limits. In Case 1, the mass of body's uncertainty is not considered. Therefore, $\Delta m_b = 0$.

Figure 2 and 3 depict the responses of the pitch angle and pitch angular velocity through the conventional and the proposed methods in Case 1, respectively. It can be seen that using the proposed method, the range of pitch angle and its velocity is smaller than those obtained through the conventional method. Figure 4 represents the wheel velocity response through conventional and proposed approach in Case 1. It shows that the wheel velocity through both control methods can reach the desired wheel velocity in a similar pattern. Figures 5 and 6 depict the response of sliding surfaces in Case 1 designed in the conventional and the proposed methods. As can be seen, all sliding surfaces converge to zero.

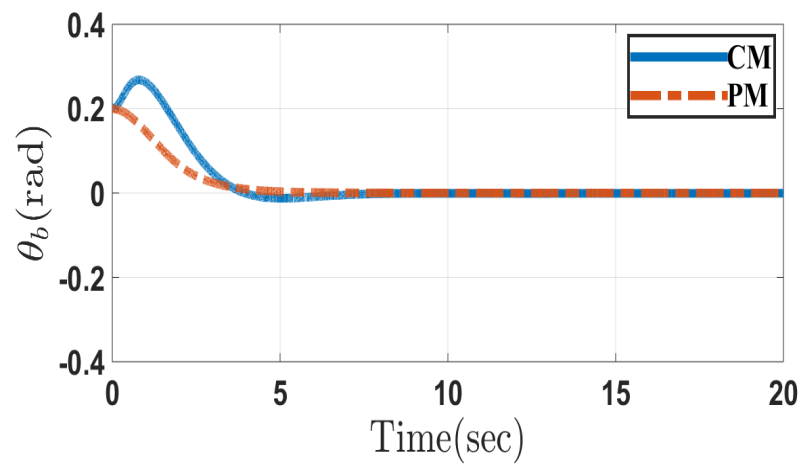


Figure 2. Pitch angle of the system in the conventional method (CM) and proposed method (PM) in Case 1.

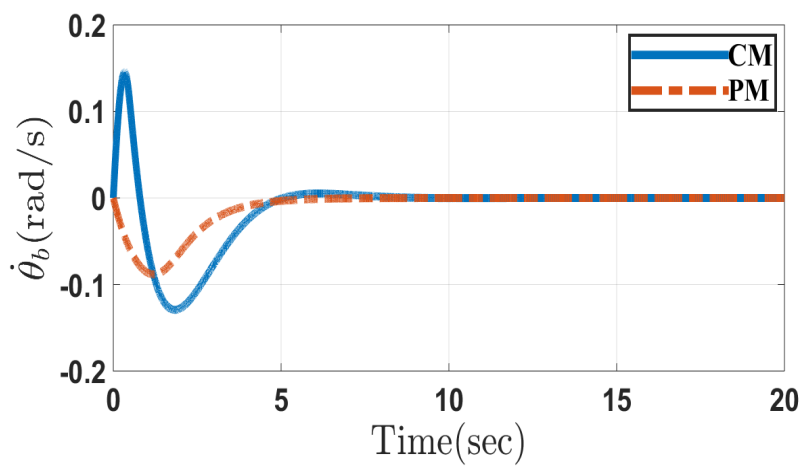


Figure 3. Pitch angular velocity of the system in the conventional method (CM) and the proposed method (PM) in Case 1.

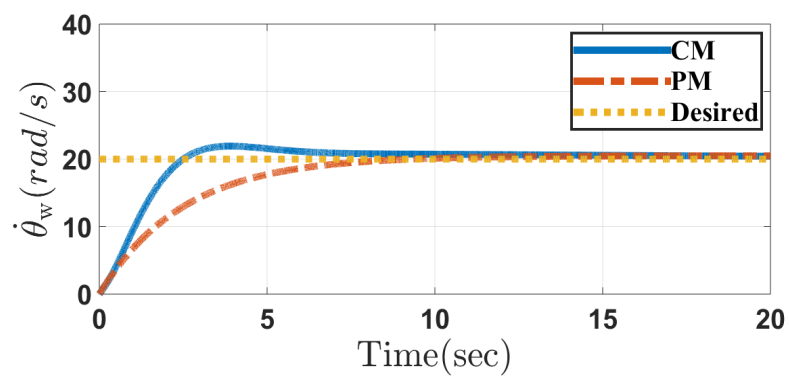


Figure 4. Wheel angular velocity of the system in the conventional method (CM) and the proposed method (PM) in Case 1.

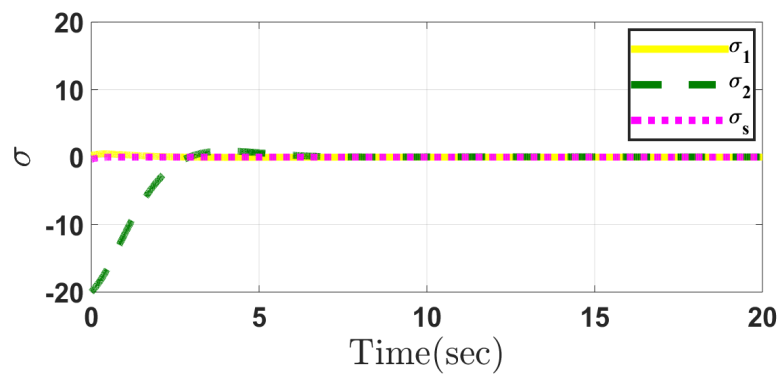


Figure 5. Sliding mode surfaces in the conventional method in Case 1.

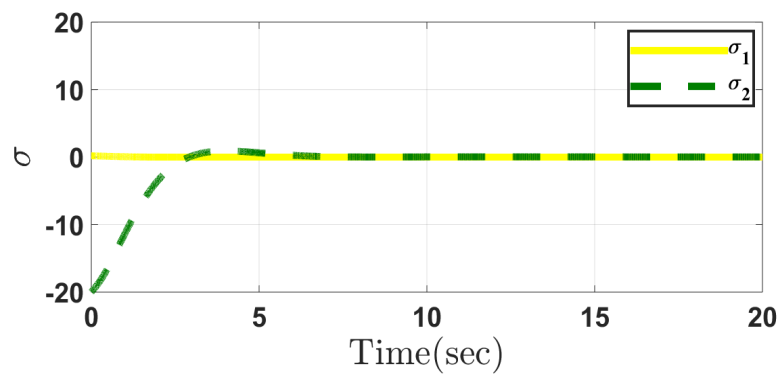


Figure 6. Sliding mode surfaces in the proposed method in Case 1.

Figure 7 depicts the input torque of wheels in Case 1 through the conventional and the proposed methods, respectively. It can be seen that they are similar to each other. However, as shown in Figure 8, the required power in the proposed method is much smaller than that required in the conventional method. There are high-frequency components in the input torque and power trajectories which are mainly due to the switching actions near the sliding surfaces in both the controllers. Though the QSMC controller is designed to smooth out the high-frequency components in the system outputs, it cannot eliminate them. On the other hand, the additional movable mechanism used in the proposed method increases the complexity of the system dynamics which also contributes to the high-frequency components.

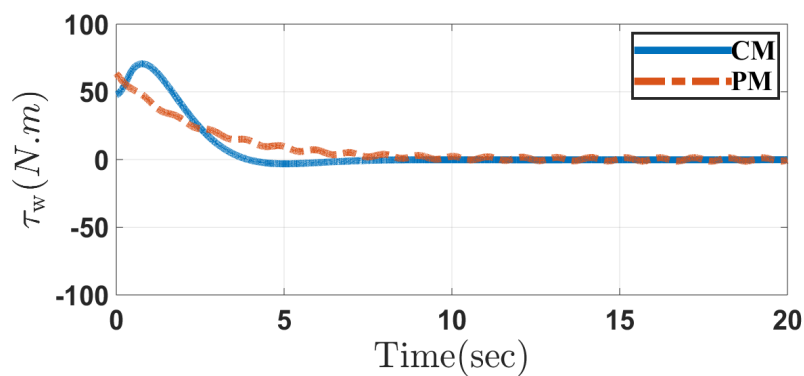


Figure 7. Input torque of wheels in the conventional method (CM) and the proposed method (PM) in Case 1.

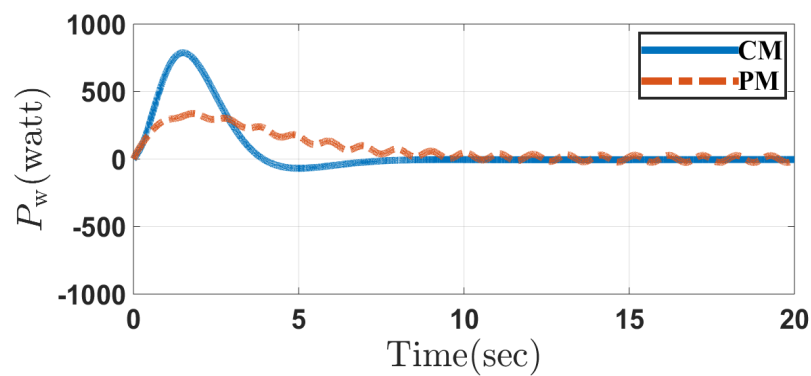


Figure 8. Input power of wheels in the conventional method (CM) and the proposed method (PM) in Case 1.

As shown in Figures 9 and 10, the input torque and power required for the motion of the pendulum is almost negligible. As shown in Figure 11, the range of the angular displacement of the pendulum is very small. This shows that it can be made compact and be operated in a small space to achieve the control objectives without causing large disturbances to the system including the rider.

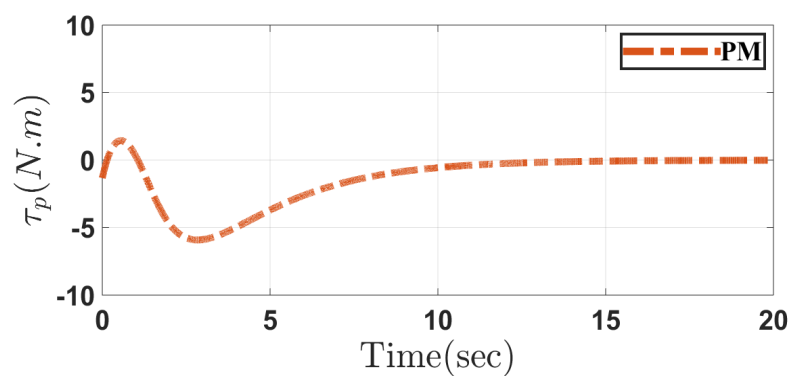


Figure 9. Input torque of movable mechanism in the proposed method (PM) in Case 1.

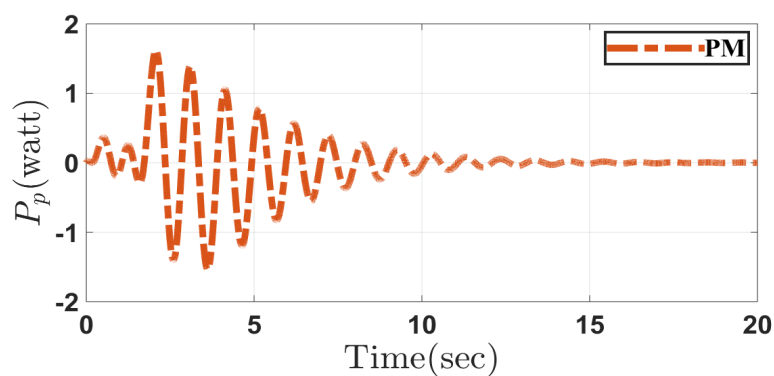


Figure 10. Input power of movable mechanism in the proposed method (PM) in Case 1.

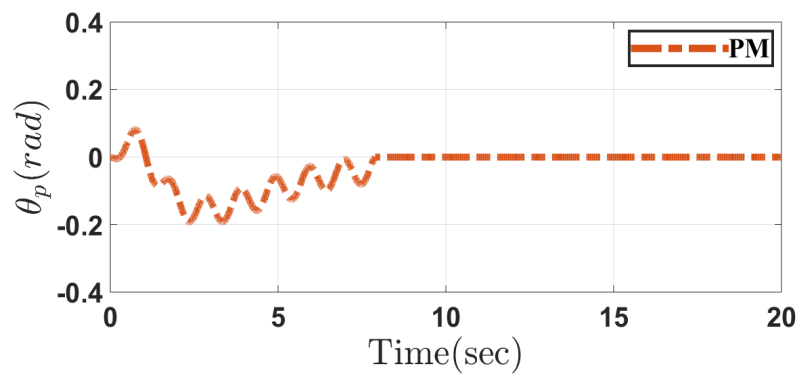


Figure 11. Movable mechanism angle in the proposed method (PM) in Case 1.

5.2. Case 2

In Case 2, the initial values of system are chosen as

$$\theta_{b_0} = 0.1 \text{ rad}, \quad \dot{\theta}_{b_0} = 0, \quad \theta_{w_0} = 0, \quad \dot{\theta}_{w_0} = 0, \quad \theta_{p_0} = 0, \quad \dot{\theta}_{p_0} = 0.$$

The control objectives are set as

$$\theta_{b_d} = 0, \quad \dot{\theta}_{b_d} = 0, \quad \dot{\theta}_{w_d} = 10 \text{ rad/s}.$$

The control parameters for the HSMC and QSMC controllers are chosen same as the values selected in Case 1. As the mass of rider varies for each person, the uncertainty of the body's mass should be considered to prove the robustness of the controllers. In this case, the uncertainty of body's mass is chosen as $\Delta m_b = 20 \text{ kg}$.

Figures 12–21 depict the performance of system in Case 2 through the conventional and proposed methods. It can be seen that the results are similar to those obtained in Case 1. Considering the disturbances caused by parameter uncertainty, the system can overcome it and prove the controller robustness designed for both the methods.

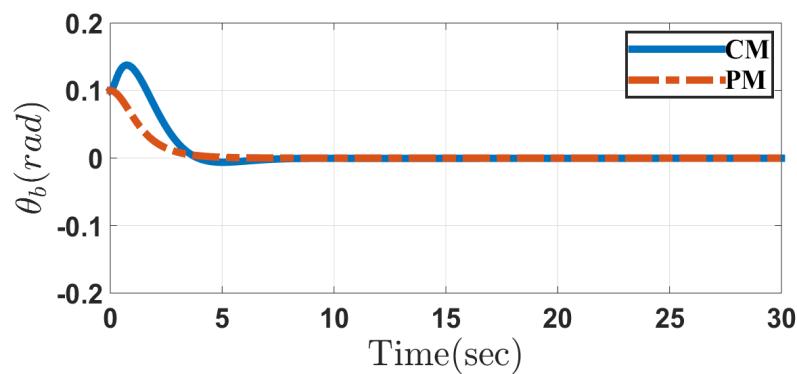


Figure 12. Pitch angle of system in the conventional method (CM) and the proposed method (PM) in Case 2.

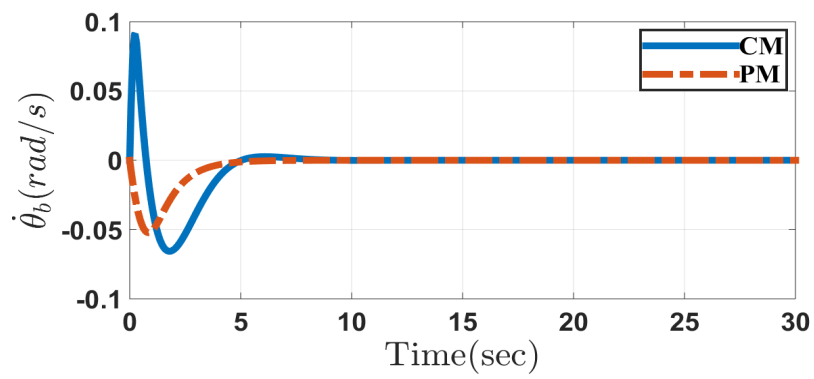


Figure 13. Pitch angular velocity of the system in the conventional method (CM) and the proposed method (PM) in Case 2.

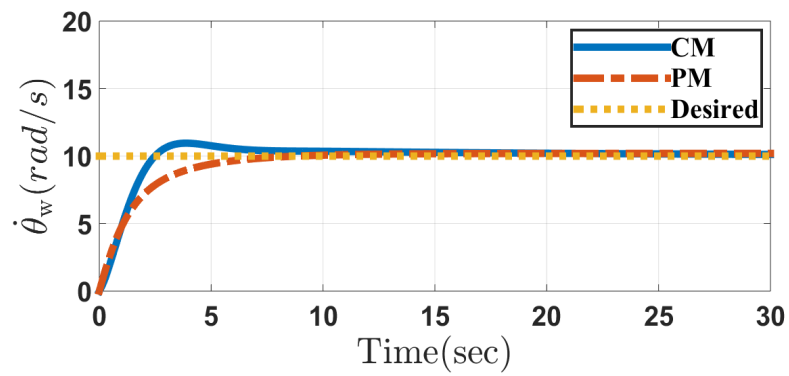


Figure 14. Wheel angular velocity of the system in the conventional method (CM) and the proposed method (PM) in Case 2.

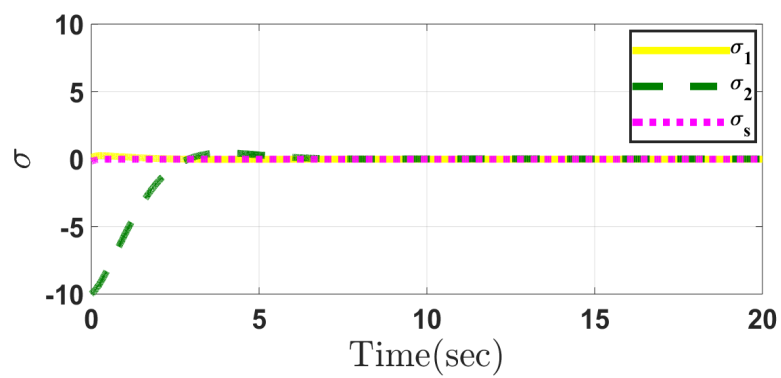


Figure 15. Sliding mode surfaces in the conventional method in Case 2.

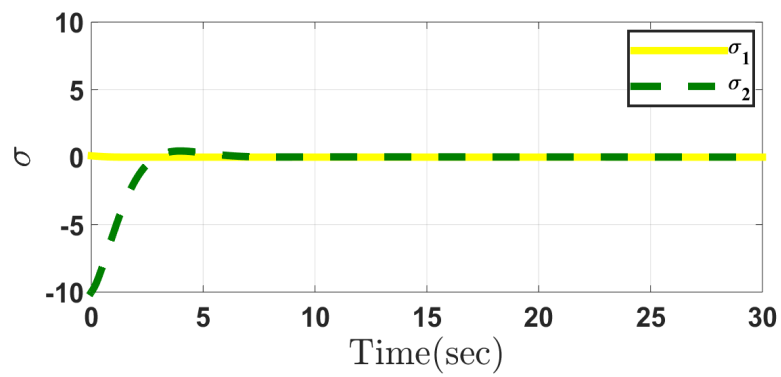


Figure 16. Sliding mode surfaces in the proposed method in Case 2.

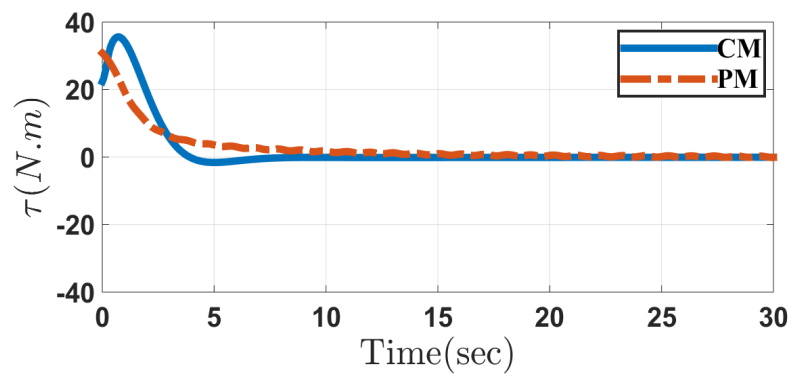


Figure 17. Input torque of the wheels in the conventional method (CM) and the proposed method (PM) in Case 2.

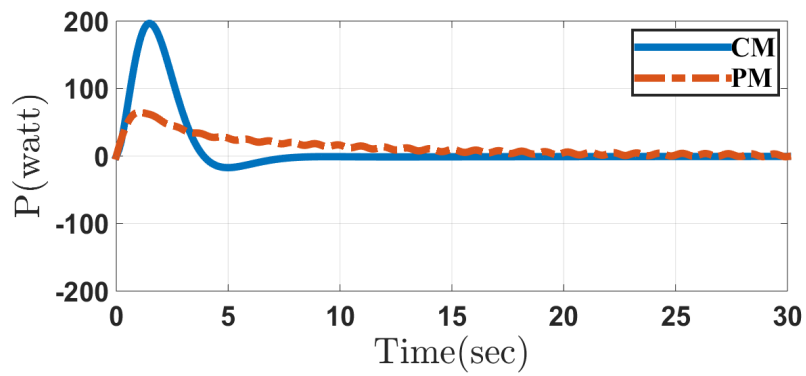


Figure 18. Input power of the wheels in the conventional method (CM) and the proposed method (PM) in Case 2.

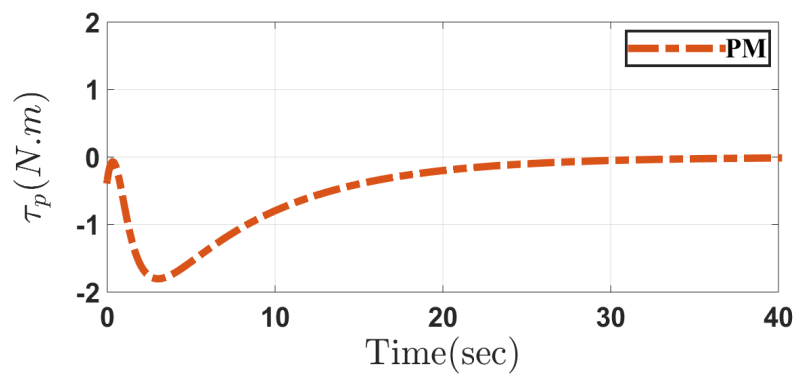


Figure 19. Input torque of the movable mechanism in the proposed method (PM) in Case 2.

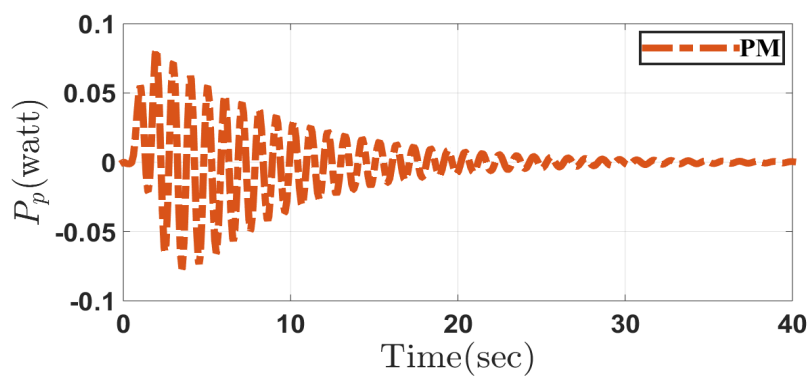


Figure 20. Input power of the movable mechanism in the proposed method (PM) in Case 2.

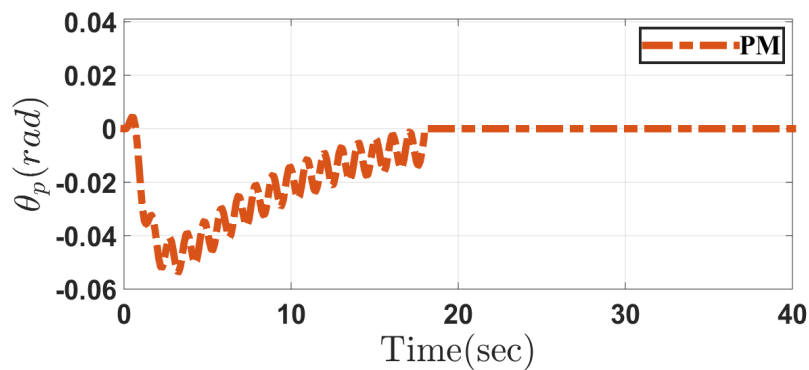


Figure 21. Movable mechanism angle in the proposed method (PM) in Case 2.

6. Conclusions

This paper presents a novel method for stability and velocity control of a two-wheeled robotic wheelchair. In this method, a movable pendulum-like movable mechanism is added to the wheelchair mainly for stability control. The Euler-Lagrange equation is used to establish the equation of motion of the system and a quasi-sliding mode control scheme is used in the controller design. The simulation results show that the proposed method achieves better stability and velocity control with less input power than the conventional methods only relying on the motions of the wheels. It is also robust against external disturbances. The future work is to implement the proposed method on a two-wheeled robotic wheelchair system under development in our lab.

Author Contributions: M.N., L.H. and A.M.A.-J. developed the idea covered in the paper; M.N. did simulations, drafted and revised the paper under the guidance of L.H. and A.M.A.-J.; L.H. is the corresponding author to revise and finalize the paper. All authors have read and agreed to the published version of the manuscript.

Funding: The project is funded by the Institute of Biomedical technologies at the Auckland University of Technology, New Zealand.

Acknowledgments: The authors would like to acknowledge Behrooz Lotfi and Simon Hartley for their advice and guidance.

Conflicts of Interest: The authors declare no conflict of interest.

Appendix A. Dynamic Model Components of Proposed Method

The $\mathbf{M}(\mathbf{q})$, $\mathbf{H}(\mathbf{q}, \dot{\mathbf{q}})$ and $\mathbf{G}(\mathbf{q})$ elements in proposed method are as below:

$$M_{11} = m_b l^2 + m_p b^2 + m_p l'^2 - 2m_p b l' \cos \theta_p + J_b + J_p, \quad M_{12} = m_b r l \cos \theta_b + m_p r b \cos \theta_b - m_p r l' \cos(\theta_b + \theta_p),$$

$$M_{13} = m_p l'^2 - m_p b l' \cos \theta_p + J_p, \quad M_{22} = (m_b + m_p + 2m_w) r^2 + 2J_w,$$

$$M_{23} = -m_p r l' \cos(\theta_b + \theta_p), \quad M_{33} = m_p l'^2 + J_p, \quad H_1 = m_p b l' (\dot{\theta}_p^2 + 2\dot{\theta}_b \dot{\theta}_p) \sin \theta_p,$$

$$H_2 = -(m_b l + m_p b) r \dot{\theta}_b^2 \sin \theta_b + m_p r l' (\dot{\theta}_b + \dot{\theta}_p)^2 \sin(\theta_b + \theta_p), \quad H_3 = -m_p b l' \dot{\theta}_b^2 \sin \theta_p,$$

$$G_1 = -m_b g l \sin \theta_b - m_p g b \sin \theta_b + m_p g l' \sin(\theta_b + \theta_p), \quad G_2 = 0, \quad G_3 = m_p g l' \sin(\theta_b + \theta_p).$$

References

1. Stout, G. Some aspects of high performance indoor/outdoor wheelchairs. *Bull. Prosthet Res.* **1979**, *16*, 135–175. [PubMed]
2. Abdulghani, M.M.; Al-Aubidy, K.M.; Ali, M.M.; Hamarsheh, Q.J. Wheelchair Neuro Fuzzy Control and Tracking System Based on Voice Recognition. *Sensors* **2020**, *20*, 2872. [CrossRef] [PubMed]
3. Ren, T.J.; Chen, T.C. Modelling and control of a power-assisted mobile vehicle based on torque observer. *IET Control Theory Appl.* **2007**, *1*, 1405–1412. [CrossRef]
4. Seki, H.; Sugimoto, T.; Tadakuma, S. Novel straight road driving control of power assisted wheelchair based on disturbance estimation and minimum jerk control. In Proceedings of the 2005 Conference Record of the Industry Applications, Fourtieth IAS Annual Meeting, Hong Kong, China, 2–6 October 2005; pp. 1711–1717.
5. Almeshal, A.M.; Goher, K.M.; Nasir, A.N.K.; Tokhi, M.O. Steering and dynamic performance of a new configuration of a wheelchair on two wheels in various indoor and outdoor environments. In Proceedings of the 2013 18th International Conference on Methods & Models in Automation & Robotics, MMAR, Miedzydroje, Poland, 26–29 August 2013; pp. 223–228.
6. Zhou, Y.; Wang, Z.; Chung, K.W. Turning Motion Control Design of a Two-Wheeled Inverted Pendulum Using Curvature Tracking and Optimal Control Theory. *J. Optim. Theory Appl.* **2019**, *181*, 634–652. [CrossRef]
7. Wieczorek, B.; Warguła, Ł.; Rybarczyk, D. Impact of a hybrid assisted wheelchair propulsion system on motion kinematics during climbing up a slope. *Appl. Sci.* **2020**, *10*, 1025. [CrossRef]
8. Hirata, K.; Murakami, T. Stability analysis of disturbance observer based controllers for two-wheel wheelchair systems. *Adv. Robot.* **2014**, *28*, 467–477. [CrossRef]
9. Vermeiren, L.; Dequidt, A.; Guerra, T.M.; Rago-Tirmant, H.; Parent, M. Modeling, control and experimental verification on a two-wheeled vehicle with free inclination: An urban transportation system. *Control Eng. Pract.* **2011**, *19*, 744–756. [CrossRef]
10. Han, J.; Li, X.; Qin, Q. Design of two-wheeled self-balancing robot based on sensor fusion algorithm. *Int. J. Autom. Technol.* **2014**, *8*, 216–221. [CrossRef]
11. Cooper, R.A.; Boninger, M.L.; Cooper, R.; Kelleher, A. Use of the INDEPENDENCE 3000 IBOT™ transporter at home and in the community: A case report. *Disabil. Rehabil. Assist. Technol.* **2006**, *1*, 111–117. [CrossRef]
12. Arthanat, S.; Desmarais, J.M.; Eikelberg, P. Consumer perspectives on the usability and value of the iBOT® wheelchair: Findings from a case series. *Disabil. Rehabil. Assist. Technol.* **2012**, *7*, 153–167. [CrossRef] [PubMed]

13. Uustal, H.; Minkel, J.L. Study of the Independence IBOT 3000 Mobility System: An innovative power mobility device, during use in community environments. *Arch. Phys. Med. Rehabil.* **2004**, *85*, 2002–2010. [\[CrossRef\]](#)
14. Baloh, M.; Parent, M. Modeling and model verification of an intelligent self-balancing two-wheeled vehicle for an autonomous urban transportation system. In Proceedings of the Conference on Computational Intelligence, Robotics, and Autonomous Systems, Singapore, 15 December 2003; pp. 1–7.
15. Karkoub, M.A.; Parent, M. Modelling and non-linear feedback stabilization of a two-wheel vehicle. *Proc. Inst. Mech. Eng. Part J. Syst. Control Eng.* **2004**, *218*, 675–686. [\[CrossRef\]](#)
16. Ghaffari, A.; Shariati, A.; Shamekhi, A.H. A modified dynamical formulation for two-wheeled self-balancing robots. *Nonlinear Dyn.* **2016**, *83*, 217–230. [\[CrossRef\]](#)
17. Nikpour, M.; Huang, L.; Al-Jumaily, A.M.; Lotfi, B. Stability control of mobile inverted pendulum through an added movable mechanism. In Proceedings of the 25th International Conference on Mechatronics and Machine Vision in Practice, M2VIP, Stuttgart, Germany, 20–22 November 2018; pp. 1–6.
18. Raffo, G.V.; Ortega, M.G.; Madero, V.; Rubio, F.R. Two-wheeled self-balanced pendulum workspace improvement via underactuated robust nonlinear control. *Control Eng. Pract.* **2015**, *44*, 231–242. [\[CrossRef\]](#)
19. Ahmad, N.S. Robust H_∞ -Fuzzy Logic Control for Enhanced Tracking Performance of a Wheeled Mobile Robot in the Presence of Uncertain Nonlinear Perturbations. *Sensors* **2020**, *20*, 3673. [\[CrossRef\]](#)
20. Raffo, G.V.; Madero, V.; Ortega, M.G. An application of the underactuated nonlinear H_∞ controller to two-wheeled self-balanced vehicles. In Proceedings of the IEEE 15th Conference on Emerging Technologies & Factory Automation, ETFA, Bilbao, Spain, 13–16 September 2010; pp. 1–6.
21. Shen, H.; Iorio, J.; Li, N. Sliding Mode Control in Backstepping Framework for a Class of Nonlinear Systems. *J. Mar. Sci. Eng.* **2019**, *7*, 452. [\[CrossRef\]](#)
22. Hong, G.S.; Yu, D.; Wong, Y.S. Integral sliding mode control for fast tool servo diamond turning of micro-structured surfaces. *Int. J. Autom. Technol.* **2011**, *5*, 4–10.
23. Nikpour, M.; Huang, L.; Al-Jumaily, A.M. Stability and Direction Control of a Two-Wheeled Robotic Wheelchair Through a Movable Mechanism. *IEEE Access* **2020**, *8*, 45221–45230. [\[CrossRef\]](#)
24. Elmokadem, T.; Zribi, M.; Youcef-Toumi, K. Control for Dynamic Positioning and Way-point Tracking of Underactuated Autonomous Underwater Vehicles Using Sliding Mode Control. *J. Intell. Robot. Syst.* **2019**, *95*, 1113–1132. [\[CrossRef\]](#)
25. Yue, M.; Wei, X. Dynamic balance and motion control for wheeled inverted pendulum vehicle via hierarchical sliding mode approach. *Proc. Inst. Mech. Eng. Part J. Syst. Control Eng.* **2014**, *228*, 351–358. [\[CrossRef\]](#)
26. Huang, J.; Guan, Z.H.; Matsuno, T.; Fukuda, T.; Sekiyama, K. Sliding-mode velocity control of mobile-wheeled inverted-pendulum systems. *IEEE Trans. Robot.* **2010**, *26*, 750–758. [\[CrossRef\]](#)
27. Huang, J.; Ding, F.; Fukuda, T.; Matsuno, T. Modeling and velocity control for a novel narrow vehicle based on mobile wheeled inverted pendulum. *IEEE Trans. Control Syst. Technol.* **2013**, *21*, 1607–1617. [\[CrossRef\]](#)
28. Sago, Y.; Noda, Y.; Kakihara, K.; Terashima, K. Parallel two-wheel vehicle with underslung vehicle body. *Mech. Eng. J.* **2014**, *1*, 1–12. [\[CrossRef\]](#)
29. Sago, Y.; Terashima, K.; Noda, Y.; Kakihara, K. Attitude control using active-mass-system in parallel two-wheel vehicle with underslung vehicle body. In Proceedings of the 2014 IEEE International Conference on Systems, Man, and Cybernetics, SMC, San Diego, CA, USA, 5–8 October 2014; pp. 1532–1537.
30. Rao, S.S.; Yap, F.F. *Mechanical Vibrations*; Prentice Hall: Upper Saddle River, NJ, USA, 2011; Volume 4.
31. Craig, J.J. *Introduction to Robotics: Mechanics and Control*; Pearson Education: Bengaluru, India, 2009; Volume 3/E.
32. Bolton, W. *Mechatronics: Electronic Control Systems in Mechanical and Electrical Engineering*; Pearson Education: London, UK, 2003.
33. Shtessel, Y.; Edwards, C.; Fridman, L.; Levant, A. *Sliding Mode Control and Observation*; Springer: New York, NY, USA, 2014.
34. Qian, D.; Yi, J. *Hierarchical Sliding Mode Control for Under-Actuated Cranes*; Springer: Heidelberg/Berlin, Germany, 2016.

